Optimization of in-depth divergence strategies

Marvin Sangers

Optimization of in-depth divergence strategies

by

Marvin Sangers

to obtain the degree of Master of Science

at the Delft University of Technology,

to be defended publicly on October 25 at 13:00.

Student number:	4227735	
Project duration:	November 16, 2017 – October 25, 2018	
Thesis committee:	Dr. O. Leeuwenburgh,	TU Delft and TNO, advisor
	Dr. D. Voskov,	TU Delft, co-advisor
	Prof. dr. P. Zitha,	TU Delft
	Prof. dr. ir. A. Heemink,	TU Delft

TU Delft

Acknowledgements

First and foremost, I would like to sincerely thank my supervisors Dr. Olwijn Leeuwenburgh and Dr. Denis Voskov for their continuous support during the course of my research. I am grateful for their insightful advice during our regular meetings. I would like to express my appreciation to Stephan de Hoop as well for his time and willingness to discus my thesis subject. Also, I would like to acknowledge the Stanford University Petroleum Research Institute for Reservoir Simulation (SUPRI-B) program for letting me use ADGPRS in this study. I cannot proceed without thanking my parents and sister for their love and support during my study. Finally I would like to thank all my friends for the great time we spent in Delft, especially Sjors with whom I enjoyed going to the gym last months.

Contents

List of Figures

List of Tables

Abstract

This study discusses the potential of the in-depth water diversion (IDD) process to enhance oil recovery from subsurface reservoirs and investigates IDD strategies through an ensemble optimization approach. Pilot studies in the North Sea performed in recent years have shown that Sodium Silicate can be applied as blocking agent, diverting water to unswept zones of the reservoir. On the other hand, numerical simulation studies have tried to simulate the IDD behaviour with methods based on weak coupling of a reservoir flow simulator and an external chemical module. This study presents a fully implicit coupled chemical-compositional-flow implementation to simulate the permeability reduction through silicate gels, since IDD is essentially a coupled flow-chemical process. In addition, this study discusses the impact of resolution in space and time on the simulation performance for 2D subsurface petroleum reservoir models. Sensitivity of the oil recovery, and IDD characteristics such as moles of silicate, to design parameters of the IDD process is discussed as well. Since adjoint gradients are not typically available for the parameters describing in-depth divergence and the uncertainties are expected to be large, the optimization study uses an ensemble-based methodology to find optimal IDD reservoir management strategies. In addition to discussing IDD strategies in a deterministic setting, the design of optimal IDD strategies under geological uncertainty is investigated. This study will demonstrate that the in-depth divergence process can be used to extend the reservoir field production life time when timing, size of the Sodium Silicate batch and concentration is optimized. Finally this study discusses the issue of computational costs associated with modeling high resolution required for accurate simulation of this coupled process.

1 Introduction

Many conventional waterflooded reservoirs are reaching their end of life with a lot of production wells producing at high water cut. Newly discovered reservoirs tend to be more complex, and therefore carry more risk and relatively high development costs. As a result, there is increased interest in Enhanced Oil Recovery (EOR) and Improved Oil Recovery (IOR) methods that can be used to extend the operating life of existing fields and increase the ultimate recovery at reasonable cost.

During waterflooding the water will tend to follow the pathway of least resistance. It may therefore predominantly flow through high permeable zones and channels, leaving other reservoir areas unswept. One option to improve the volumetric sweep efficiency is the use of IOR methods such as in-depth water divergence (IDD). Green chemicals, such as the PLONOR listed chemical sodium silicate (Hatzignatiou et al. (2016)), should make these methods more attractive for wide-scale employment. Sodium silicate can potentially flow for a long distance, far away from the injector, to a place where it forms a gel under certain activation conditions, either thermal or chemical. As such a gel has the ability to withstand large pressure gradients it can divert injected water to unswept zones (Skrettingland et al. (2016)).

A number of pilot studies in the North Sea have demonstrated in recent years that sodium silicate can be successfully employed to enhance recovery from producing fields (Skrettingland et al. (2012, 2014)). Combined with these pilots, experimental laboratory work has given insight on activation conditions, core-scale behaviour, and chemistry of the poorly understood polymerization process (Icopini et al. (2005); Stavland et al. (2011)). Several numerical simulation studies, based on a weak coupling of a reservoir flow modeling and a separate software module for chemical reactions, have been able to replicate the main characteristics of the observed behaviour (Hiorth et al. (2016); Skrettingland et al. (2014)). Since the development of silicate gels and the accompanying permeability reduction is essentially a coupled process, Trujillo et al. (2018) recently proposed a fully implicit coupled chemical-compositional-flow implementation.

The success of an IDD process depends on complex interactions between multiple parameters, and only some of them are under the control of an operator. In the first stage of the IDD process, a pre-flush volume of Potassium Chloride (KCL) brine is injected to act as a stabilizer, preventing clay swelling and rapid plugging due to mineral precipitation (Skrettingland et al. (2014)). The operator can furthermore control the timing and duration (or volume) of the sodium silicate slug, and the concentration of the solution. Other aspects of the IDD process are more complex to control or poorly understood. Stavland et al. (2011) mention the pH changes within the reservoir due to complex chemical reactions taking place. Low pH can result in a short gelation time and therefore alkaline gels are preferred over acidic gels, despite having a lower gel strength (Hamouda and Amiri (2014)). Additionally Trujillo (2017) indicates that the particle size is a key parameter in the reduction of porosity and permeability, where the Icopini et al. (2005) reaction model with low concentration rates is the best suitable for simulation purposes.

The resulting difficulty of designing a good operational strategy suggests that optimization methods can help identifying a good (or even optimal) strategy. To the best of my knowledge, optimization of IDD involving tuning of the silica injection parameters and treatment of upscaling effects in reactive transport for the IDD process has not previously been performed. This thesis intends to investigate if such a model-based approach could be feasible.

There are some challenges related to the correct simulation of the gelation process. Trujillo et al. (2018) mention the scale dependence of the kinetic rate. The physics of the silica reaction kinetics occur in the local domain and much faster than the transport phenomena in the global domain. The high order reaction rate of concentration suggests the need for upscaling this complexity. A proper choice for the simulation scale parameters will therefore contribute to the performance of any optimization exercise.

Different optimization methods exist to find possible proactive reservoir management strategies and these can be divided into two main categories according to Hou et al. (2015): gradient-free and gradient-

based methods. Jansen (2011) provides an extensive review on the adjoint-based optimization method, which acquires gradient information from a co-state equation. Although being the most accurate and efficient way to compute the gradient for a large number of controls, the adjoint is intrusive and difficult to implement in existing simulation programs. For controls describing the IDD process, it's likely exact gradients do not exist making the adjoint method unattractive. Alternatives are methods which approximate the gradient, such as Simultaneous Perturbation Stochastic Approximation (*SPSA*) Spall (1998) and Ensemble based Optimization (*EnOpt*) Chen (2008); Fonseca et al. (2017). Ensemble based Optimization has found to be efficient when dealing with uncertain models and it has been shown to acquire good results in a wide scale of reservoir models (Fonseca et al. (2014a)), making it suitable for optimization of the IDD process. Simulated Annealing Metropolis et al. (1953) and Particle Swarm Optimization Kennedy (2011) are methods part of the gradient-free methods.

1.1 Objectives and problem definition

This thesis objectives are (1) to create relevant reservoir test cases of increasing complexity in structure and heterogeneity as setting for in depth divergence and (2) to modify and use the *EnOpt* optimization workflow to determine the potential to increase value by in depth divergence.

Following from the issues related to the success of an IDD process are a number of research questions, such as: (1) How can the in-depth diversion process be parameterized in terms of controls that make it suitable for optimization? (2) To what extent is upscaling required to make the optimization computationally tractable? Which are efficient and effective upscaling strategies, and how can they be incorporated into the optimization workflow? (3) What is the scope for IDD strategies to improve recovery of oil or economic performance (NPV)?

1.2 Hypothesis

"Ensemble-based optimization techniques can be used to identify in-depth diversion strategies that lead to significantly improved recovery of subsurface resources".

1.3 Thesis outline

This thesis focuses on the impact of the spatial and temporal resolution of the simulations, and on the potential to use the simulations to find operational IDD strategies (timing, duration and concentration of the sodium silicate solution slug) that deliver improved performance over conventional waterflooding strategies. For enhanced realism the presence of geological uncertainty is considered and an ensemble of geological realizations is used to represent this uncertainty. This thesis demonstrates that the resulting optimal strategy is non-trivial and differs from a normal reactive approach, where the injection is started immediately after water breakthrough.

The remainder of this thesis starts with a theoretical background, followed by a discussion of the modeling approach and a brief description of the IDD simulation process. Subsequently, this thesis describes the optimization formulation based on an ensemble approach. Several numerical experiments are presented based on a simple 2D model representing a layered vertical reservoir cross-section connecting an injection and production well. Lastly, results are presented on the sensitivity to model parameters and applications of an optimization methodology to both a synthetic layered model and a channelized reservoir, ending with some conclusions.

2 Ensemble optimization theory

This chapter provides a theoretical background on ensemble optimization. First, the main optimization algorithm is discussed, together with two common control updating strategies. These strategies are the line search and trust region algorithm. Then, both deterministic ensemble optimization and ensemble optimization under uncertainty are discussed.

2.1 Optimization algorithm

Optimization approaches can be subdivided into gradient- and gradient free methods. Gradient free methods are especially useful when handling discrete controls and discontinuous functions and even a certain amount of noise. The major disadvantage is the amount of time it takes to handle a large number of variables, making these methods computational expensive. An alternative are gradient based optimization methods, such as the adjoint method.

The adjoint optimization method is the most accurate for gradient computation, but will require full access to the simulator source code. Access to this code is often not possible in commercial simulators and therefore the adjoint method is more suitable for in-house developed simulators. The implementation of the adjoint is time consuming when complexity of physics increases. Stochastic optimization methods don't need access to the source code and therefore treat the simulator as a black box. One of these methods is the Ensemble Optimization method (EnOpt), which relies on perturbed control vectors to estimate gradients.

The EnOpt algorithm is an iterative process consisting of inner and outer iterations. In the outer iteration the gradient will be evaluated for the current controls and a search direction is calculated. Now within the outer iteration, an inner iterations starts. In this inner iteration a control update is proposed and the objective function is re-evaluated and checks if there is an acceptable increase in objective function. If this is not acceptable, either the trust region step or line search step is adjusted and a new control update is proposed, which will be a new inner iteration. If this increase is acceptable the inner iteration stops and the outer iteration continues with the best result from the inner loop, to do a new evaluation of the gradient with the control updates leading to a new outer iteration.

Two common strategies exist in the optimization algorithm to move from the current control set to an updated control set: line search and trust region.

2.1.1 Line Search algorithm

Line search first finds a search direction $\boldsymbol{s}$ and then along this direction a suitable step size is chosen. The search direction is typically the gradient itself. It can also be scaled version of the gradient to enable large steps close to control boundaries $\boldsymbol{u}_{\max}$ and $\boldsymbol{u}_{\min}$, according to

$$s_i = \begin{cases} s_i \cdot (u_i^{\max} - u_i) & \text{if } s_i > 0 \\ s_i \cdot (u_i^{\min} - u_i) & \text{if } s_i < 0 \end{cases} \tag{1}$$

Outward pointing gradients for controls at the bounds can be set to zero. Determination of the step size is done using trial sizes and one of them will be accepted if some conditions are met. A trial step size is rejected when it results in a non-increase of the objective function J. Most likely the initial guess for this step size was too large and therefore the next guess will be smaller. In determination of the trial step size one can impose three upper bounds: l^f, l^J and l^u. The first bound will be imposed on the feasible domain, the second on the objective function and the last bound on the controls:

1. The solution should lie in the feasible domain: $\boldsymbol{u}^{\min} \leq \boldsymbol{u} + l \cdot \boldsymbol{s} \leq \boldsymbol{u}^{\max}$.

$$l_i^f = \begin{cases} \left(\frac{u_i^{\max} - u_i}{s_i}\right) & \text{if } s_i > 0 \\ \left(\frac{u_i^{\min} - u_i}{s_i}\right) & \text{if } s_i < 0 \\ \text{very large number} & \text{else} \end{cases} \tag{2}$$

   Equation 3 takes the minimum step size from the vector elements in 2 as the upper bound for the feasible domain.

$$l^f = \min_{i=1:n} f_i^f \tag{3}$$

2. There exist a maximum to the expected increase in objective function, given by a fraction c_1 which is the relative increase: $l^J \cdot (J(\boldsymbol{u} + l \cdot \boldsymbol{s}) - J(\boldsymbol{u})) \leq (c_1 + 1) \cdot (|J(\boldsymbol{u})| + 1)$. Then equation 4 gives the second upper bound.

$$l^J = \frac{(c_1 + 1)\,(|J(\boldsymbol{u})| + 1)}{\boldsymbol{g}^T \boldsymbol{s}} \tag{4}$$

3. The relative change in control values has an upper bound as well: $||\boldsymbol{u} + l \cdot \boldsymbol{s}|| \leq (c_2 + 1) \cdot ||\boldsymbol{u}||$. Then 5 results in the third upper bound.

$$l_i^u = \frac{c_2 ||\boldsymbol{u}||}{||\boldsymbol{s}||} \tag{5}$$

The maximum step size l will be the most restrictive one, based on the three imposed upper bounds, according to 6.

$$l = \min\left(l^f, l^J, l^u\right). \tag{6}$$

One of the Wolfe conditions is the Armijo condition 7, which guarantees a sufficient increase in the objective function value where $0 < c_w < 1$ is the Wolfe constant. R is the ratio of the actual increase and predicted increase in objective function value J

$$R = \frac{J^{\text{new}} - J^{\text{old}}}{J(\boldsymbol{u} + l \cdot \boldsymbol{s}) - J(\boldsymbol{u})} = \frac{J^{\text{new}} - J^{\text{old}}}{\boldsymbol{g}^T \boldsymbol{s}} \geq c_w l \tag{7}$$

If this condition is satisfied, then the inner loops stops. Otherwise the step size l will be multiplied with a predefined contraction factor and a new inner iteration begins.

2.1.2 Trust Region algorithm

The trust region method makes use of a model function f with similar behaviour as the objective function near the the point $\boldsymbol{u}_k$. In this study, the model function is a first order Taylor expansion of the objective function around $\boldsymbol{u}_k$, where $\boldsymbol{u}_k + \boldsymbol{s}$ lies inside the trust region.

$$\max_{\boldsymbol{s}} f(\boldsymbol{u}_k + \boldsymbol{s}) = \max_{\boldsymbol{s}} J(\boldsymbol{u}_k + \boldsymbol{s}) = J(\boldsymbol{u}_k) + \boldsymbol{g}_k^T \boldsymbol{s} \tag{8}$$

$$\text{s.t. } ||\boldsymbol{s}||_\infty < \tau \cdot (\boldsymbol{u}^{\max} - \boldsymbol{u}^{\min}) \quad \text{and} \quad \boldsymbol{u}^{\min} \leq \boldsymbol{u}_k \leq \boldsymbol{u}^{\max}, \tag{9}$$

The trust region based search vector $\boldsymbol{s}$ is determined using 10. If the original search direction is positive, then the new search direction will be the minimum of the distance to the bounds and the trust size factor multiplied by the difference between the maximum and the minimum of the control. If it is negative, then it will be the maximum. If the difference between the new and old search direction is close to some tolerance, the new search direction will be set to zero.

$$s_i = \begin{cases} \min\left[(u_i^{\max} - u_i), \tau\left(u_i^{\max} - u_i^{\min}\right)\right] & \text{if } g_i > 0 \\ \max\left[\left(u_i^{\min} - u_i\right), -\tau\left(u_i^{\max} - u_i^{\min}\right)\right] & \text{if } g_i < 0 \\ 0 & \text{if } g_i = 0. \end{cases} \tag{10}$$

$$R = \frac{J^{\text{new}} - J^{\text{old}}}{J(\boldsymbol{u}_k + \boldsymbol{s}) - J(\boldsymbol{u}_k)} = \frac{J^{\text{new}} - J^{\text{old}}}{\boldsymbol{g}^T \boldsymbol{s}} \tag{11}$$

Just like the line search method, the ratio R of the actual increase and predicted increase in objective function value can be used for making a decision if model f should be trusted. To make a decision, a minimum r_1 and maximum r_2 ratio of the actual increase and predicted increase in objective function value is used.

$$\begin{bmatrix} ts, & \text{stop} \end{bmatrix} = \begin{cases} \begin{bmatrix} f_{\text{contraction}} \cdot ts, & \text{No} \end{bmatrix} & \text{if } R < r_1 \\ \begin{bmatrix} ts, & \text{Yes} \end{bmatrix} & \text{if } r_1 \leq R < r_2 \\ \begin{bmatrix} \min(f_{\text{expansion}} \cdot ts, t_{\max}), & \text{Yes} \end{bmatrix} & \text{if } R \geq r_2 \end{cases} \tag{12}$$

If $R < r_1$, the model is not trusted and the trust size is multiplied with a contraction factor and the inner loop does not stop. It stops if $r_2 > R \geq r_1$ and the model is trusted or if $R \geq r_2$, then the trust region will be expanded.

2.1.3 Inner and Outer iterations

In Ensemble Optimization methods there are two types of iterations: Inner and Outer. In the outer iteration the objective function and gradient are evaluated and a search direction $\boldsymbol{s}$ is calculated. For the trust region the update step is an adjusted search direction and for the line search method the update step is a step length.

Then, within the outer loop, an inner loop starts where a control update is proposed. If the trust region method was used, this update is $\boldsymbol{u} = \boldsymbol{u}_0 + \boldsymbol{s}$. For the line search method, the update to the controls is $\boldsymbol{u} = \boldsymbol{u}_0 + l \cdot \boldsymbol{s}$. The objective function is re-evaluated and the inner loop stops if there is a reasonable increase in objective function J or if the maximum allowed inner iterations is reached. If there is not enough increase in J, there will be another inner iteration where either the trust size or the step length is decreased.

Exiting the inner loop, the outer iteration continuous with accepting the current controls. It will re-evaluate the gradient and objective function and continue to the next outer iteration. This outer loop stops if there is no more significant improvement in objective function value during three outer iterations or if the maximum allowed number of outer iterations is reached.

2.2 Deterministic Ensemble Optimization

The process is said to be deterministic when there is only one model realization used to represent the geology, i.e there is no uncertainty in geological parameters. The optimization process is controlled by an input or control vector $\boldsymbol{u}$ of length N, where N is the number of control variables n times the number of control time steps t. The derivation below of the deterministic EnOpt is based on Leeuwenburgh (2017).

$$\boldsymbol{u} = [\boldsymbol{u}_{t=1}^T, \boldsymbol{u}_{t=2}^T, \ldots, \boldsymbol{u}_{t=t_{\text{end}}}^T]^T = [u_1, u_2, \ldots, u_N]^T \tag{13}$$

A first order Taylor series expansion of the objective function behavior can give a approximation of the gradient 14, with α being a scalar multiplier.

$$J(\boldsymbol{u}_k + \alpha \delta \boldsymbol{u}) = J(\boldsymbol{u}_k) + \alpha \delta \boldsymbol{u}^T \nabla J + \mathcal{O}(\alpha^2) \tag{14}$$

Improvement in the objective function $J(\boldsymbol{u}_{k+1}) > J(\boldsymbol{u}_k)$ is there only when $\alpha \delta \boldsymbol{u}^T \nabla J > 0$ in each iteration step k. The ensemble of perturbation directions $\delta \boldsymbol{u}^i = \boldsymbol{u}_k^i - \boldsymbol{u}_k$ for $i = \{1, \ldots, N_p\}$ is sampled from a Gaussian distribution $\mathcal{N}(0, C_{uu})$, with N_p the total number of pertubations. The objective function changes value according to these perturbations, which can be used to approximate the gradient $\boldsymbol{g} = \nabla J_k$.

$$\delta J_k^i = J(\boldsymbol{u}_k^i) - J(\boldsymbol{u}_k) \approx \delta \boldsymbol{u}^{iT} \boldsymbol{g} \tag{15}$$

In matrix form $\mathrm{U}\boldsymbol{g} = \boldsymbol{j}$:

$$\begin{bmatrix} u^1_{1,k} - u_{1,k} & \dots & u^1_{N,k} - u_{N,k} \\ \vdots & \ddots & \vdots \\ u^{N_p}_{1,k} - u_{1,k} & \dots & u^{N_p}_{N,k} - u_{N,k} \end{bmatrix} \begin{bmatrix} g_{1,k} \\ \vdots \\ g_{N,k} \end{bmatrix} = \begin{bmatrix} J(\boldsymbol{u}^1_k) - J(\boldsymbol{u}_k) \\ \vdots \\ J(\boldsymbol{u}^{N_p}_k) - J(\boldsymbol{u}_k) \end{bmatrix} \tag{16}$$

where $\mathrm{U} = N_p \times N$, $\boldsymbol{g} = N \times 1$ and $\boldsymbol{j} = N_p \times 1$. To reduce computation time the case $N_p < N$ is interesting, resulting in an under determined system of equations. The gradient is then computed with the pseudo inverse and using singular value decomposition (SVD).

$$\mathrm{U} = \begin{bmatrix} \mathrm{D}_p & \mathrm{D}_0 \end{bmatrix} \begin{bmatrix} \Lambda_p & 0 \\ 0 & 0 \end{bmatrix} \begin{bmatrix} \mathrm{V}^T_p \\ \mathrm{V}^T_0 \end{bmatrix} = \mathrm{D}_p \Lambda_p \mathrm{V}^T_p \tag{17}$$

With property $(\mathrm{V}_p \Lambda_p^{-1} \mathrm{D}^T_p)(\mathrm{D}_p \Lambda_p \mathrm{V}^T_p) = \mathrm{I}$ gives solution 18.

$$\boldsymbol{g} = (\mathrm{U}^T\mathrm{U})^+ \mathrm{U}^T \boldsymbol{j} = \mathrm{U}^+ \boldsymbol{j} = \mathrm{V}_p \Lambda_p^{-1} \mathrm{D}^T_p \boldsymbol{j} = \sum_{i=1}^{p} \left(\frac{\boldsymbol{d}_i^T \boldsymbol{j}}{\lambda_i} \boldsymbol{v}_i \right) \tag{18}$$

When sampling from a $\mathcal{N}(0, C_{uu})$ Gaussian distribution gradient $\boldsymbol{g}$ can be written in terms of the sample based approximation of the covariance matrix: it is then the product of the inverse auto covariance matrix of the control perturbations with the cross covariance matrix between the control and the objective function perturbation 19.

$$\boldsymbol{g} = \mathbb{E}\left[\left(\frac{1}{N_p} \sum_{i=1}^{N_p} \delta \boldsymbol{u}^i (\delta \boldsymbol{u}^i)^T \right)^+ \left(\frac{1}{N_p} \sum_{i=1}^{N_p} \delta \boldsymbol{u}^i \delta J^i \right) \right] = (\hat{C}_{uu})^+ \hat{C}_{uJ} \tag{19}$$

2.3 Ensemble Optimization under Uncertainty

Deterministic optimization is only useful when the uncertainty in geological parameters is small and only one model is used to capture these properties. In reality, multiple geological models are used to represent the uncertainty in the reservoir model and optimization of one model is not sufficient to come up with the optimal strategy.

To account for geological uncertainty, an ensemble of M reservoir models can be used, each having a vector $\boldsymbol{m}$ with uncertain reservoir model parameters in addition to the ensemble of perturbed control directions 20. In this study the uncertain model parameter will be permeability (and porosity).

$$\boldsymbol{m} = [(\boldsymbol{m}_{l=1})^T, (\boldsymbol{m}_{l=2})^T, \dots, (\boldsymbol{m}_{l=M})^T]^T \tag{20}$$

Instead of maximizing a deterministic objective function, the expected value of the objective function will be maximized which is the average of the gradients for each geological model.

$$\bar{J}(\boldsymbol{u}, \boldsymbol{m}) = \frac{1}{M} \sum_{l=1}^{M} J(\boldsymbol{u}, \boldsymbol{m}_l) \tag{21}$$

To evaluate 21, one needs $N_{\text{total}} = M * N_p$ function evaluations, too much for normal computation scenarios. Chen et al. (2009) came up with a way to reduce computation time by pairing each control with one single geological model and allowing the number of simulations to scale linearly with them. Fonseca et al. (2017) argues that one of the assumptions required with the original EnOpt method of Chen et al. (2009) conflicts with the main interest of incorporating geological uncertainty.

$$\bar{J}(\boldsymbol{u}_k, \boldsymbol{m}) = \frac{1}{N_p} \sum_{i=1}^{N_p} J(\boldsymbol{u}^i_k, \boldsymbol{m}_i) \approx J(\bar{\boldsymbol{u}}_k, \boldsymbol{m}) \approx J(\boldsymbol{u}_k, \boldsymbol{m}) \tag{22}$$

Assumption 22 would then suggest $J(\boldsymbol{u}_k, \boldsymbol{m}_1) \approx \ldots \approx J(\boldsymbol{u}_k, \boldsymbol{m}_M)$ and this holds only when the variance between the different geological models is very small. Without the need to make this assumption, Fonseca et al. (2017) introduced the StoSAG search direction method as a better alternative to the original EnOpt. The objective function anomaly accounting for uncertainty can be written as:

$$\boldsymbol{j} = \left[J\left(\boldsymbol{u}_k^1, \boldsymbol{m}_l\right) - J\left(\boldsymbol{u}_k, \boldsymbol{m}_l\right) \quad \ldots \quad J(\boldsymbol{u}_k^{N_p}, \boldsymbol{m}_l) - J\left(\boldsymbol{u}_k, \boldsymbol{m}_l\right) \right]^T \tag{23}$$

A first order Taylor expansion of the objective function will have the form of equation 24.

$$J\left(\boldsymbol{u}_k^i, \boldsymbol{m}_l\right) - J\left(\boldsymbol{u}_k, \boldsymbol{m}_l\right) = \left(\boldsymbol{u}_k^i - \boldsymbol{u}_k\right)^T \nabla_u J\left(\boldsymbol{u}_k, \boldsymbol{m}_l\right) + \text{HOT} \tag{24}$$

Equation 24 can be used to write the sample approximation of the cross covariance matrix between the controls and the mean objective function, where $\bar{\boldsymbol{g}} = \frac{1}{M} \sum_{l=1}^{M} \nabla_u J\left(\boldsymbol{u}_k, \boldsymbol{m}_l\right)$.

$$\hat{C}_{u\bar{J}} = \mathbb{E}\left[\frac{1}{M} \sum_{l=1}^{M} \frac{1}{N_p} \sum_{i=1}^{N_p} \left(\boldsymbol{u}_k^i - \boldsymbol{u}_k\right) \left(J\left(\boldsymbol{u}_k^i, \boldsymbol{m}_l\right) - J\left(\boldsymbol{u}_k, \boldsymbol{m}_l\right) \right) \right] \tag{25}$$

$$= \frac{1}{M} \sum_{l=1}^{M} \left(\frac{1}{N_p} \sum_{i=1}^{N_p} \mathbb{E}\left[\left(\boldsymbol{u}_k^i - \boldsymbol{u}_k\right) \left(\boldsymbol{u}_k^i - \boldsymbol{u}_k\right)^T \right] \nabla_u J\left(\boldsymbol{u}_k, \boldsymbol{m}_l\right) \right) \tag{26}$$

$$= \hat{C}_{uu} \left(\frac{1}{M} \sum_{l=1}^{M} \nabla_u J\left(\boldsymbol{u}_k, \boldsymbol{m}_l\right) \right) = \hat{C}_{uu} \bar{\boldsymbol{g}} \tag{27}$$

The gradient is now written in terms of the covariance matrix accounting for geological uncertainty, similar to the deterministic case.

$$\bar{\boldsymbol{g}} = \hat{C}_{uu}^{+} \hat{C}_{u\bar{J}} \tag{28}$$

3 Modeling approach

In this section, the major ingredients are described of the modeling approach used for this study. For further details of the implementation the reader is referred to Trujillo et al. (2018).

3.1 In-depth water diversion simulation

Trujillo et al. (2018) adapted and validated the Hiorth et al. (2016) porosity-permeability model and the 4-component silica gelation reaction suggested by Icopini et al. (2005) for in-depth divergence simulation. These models were implemented in the Automatic Differentiation General Purpose Research Simulator (AGGPRS) developed at Stanford University (Voskov and Tchelepi, 2012; Zaydullin et al., 2014; Garipov et al., 2018). The governing equations for reactive flow and transport, as implemented in ADGPRS (Farshidi et al., 2013; Voskov et al., 2017), involve generic conservation of mass of species

$$\frac{\partial n_i}{\partial t} + l_c + q_c = \sum_{k=1}^{K} v_{ck} r_k + \sum_{q=1}^{Q} v_{cq} r_q, \quad c = 1, \ldots, C, \tag{29}$$

where n_c is the overall mass of component, l_c is the total flux associated with that component, v_{ck} is the stoichiometric coefficient associated with kinetic reaction k for the component c and v_{cq} is the stoichiometric coefficient associated with equilibrium reaction q for component c. r_k is the rate for kinetic reaction k and r_q is the rate for equilibrium reaction q. In this study, kinetic reactions describe the complicated gelation process as suggested in Trujillo et al. (2018).

The assumption is solid species of the reaction are not transported, but deposited as a gel within the matrix. This deposited gel will then decrease porosity. As mentioned earlier, the 4-component reaction for modeling the polymerization process is used (Trujillo et al., 2018),

$$H_8Si_3O_{10(\mathrm{aq})} + H_4\mathrm{Si}O_{4(\mathrm{aq})} \xrightarrow{k_1} H_8Si_4O_{12(\mathrm{gel})} + 2H_2O \tag{30}$$

Icopini et al. (2005) reported a fourth order reaction rate (31) of the concentration for the consumption of H_4SiO_4.

$$\frac{dc}{dt} = -k\,c^4 \quad , \tag{31}$$

where c is the concentration of $H_4\mathrm{Si}O_{4(\mathrm{aq})}$. The change of porosity is related to the molar deposition of the solid species according to

$$\phi(t) = 1 - C_{rock} - \frac{N_{solid}(t) \times M_{v_{solid}}}{V_{cell}} \quad , \tag{32}$$

where N_{solids} is the amount of moles of solids deposited, $M_{v_{solid}}$ is the molecular volume of the solid, V_{cell} the cell volume, and C_{rock} the fraction of rock. Finally, the Hiorth et al. (2016) pore throat blockage model (33) approximates permeability as function of initial permeability k_0 and porosity φ_0, the mass fraction of deposited silica over water Y and the water saturation S_w,

$$k = k_o \left(1 + 275 Y S_w \sqrt[2]{\frac{k_o}{\phi_o}}\right)^{-2} \quad . \tag{33}$$

3.2 Optimization formulation

The primary objective in the exploitation of oil reservoirs is normally to maximize economic value, where value is generally dominated by the revenues associated with increased oil recovery. One way to improve oil recovery is to implement smart injection and production strategies. Such strategies can be found with the help of simulation models and numerical optimization techniques. A waterflood strategy, for example, is characterized by time series of injection and production rates, or bottom hole pressures,

in all wells. These so-called controls can be manipulated such that a user-specified objective function, that can be evaluated from the model output, is maximized.

When IDD is implemented to further increase recovery, an additional set of controls should be included. Here, this study considers the start time for the injection of the silicate slug, the slug size, and the silicate concentration as the control variables. The slug size will be defined in terms of the injection duration in days. In order to determine the economic value of the project, the objective function is net present value (NPV) which is computed as the integral over all timesteps $n = \{1,\ldots,N\}$ of the discounted cash flow incurred in each time step.

This cash flow is obtained as the product of production and injection rates of oil (Q_o), water (Q_{wi} and Q_{wp}) and silicate (Q_c) with the associated prices per unit volumes (r_o, r_{wi}, r_{wp}, and r_c) respectively, and the time step interval Δt. The subscript o stands for oil, wi for water injected, wp for water produced, and c for the injected sodium silicate. The discount factor b per time interval τ is used to include the time value of money. With these definitions the objective function becomes

$$J = \sum_{k=1}^{K} \left[\frac{(Q_o \cdot r_o - Q_{wp} \cdot r_{wp} - Q_{wi} \cdot r_{wi} - Q_c \cdot r_c) \cdot \Delta t}{(1+b)^{(t/\tau)}} \right]. \tag{34}$$

The values of the fixed prices that are used in this study are listed in Table 1. The cost of the injected

Notation	Value	Unit
r_o	150	$\$/m^3$
r_{wp}	25	$\$/m^3$
r_{wi}	5	$\$/m^3$
b	0 and 8	%/year

Table 1 *Prices per injected or produced volume and discount rate used in this paper.*

silicate solution r_{ci} is expressed as a function of the silicate concentration in water (35). With C being the concentration in wt% and P the price of dry sodium metasilicate in $\$/m^3$, the cost per unit volume of concentrate is

$$r_{ci} = P \cdot \frac{C}{100} + r_{wi} \cdot \frac{100 - C}{100}. \tag{35}$$

Mayer et al. (1983) reported a price range of 310 - 415 USD per dry ton sodium metasilicate (Na_2SiO_3, 2.4 g/cm^3), equivalent to $P = 820$ USD per m^3. For the simple cases considered in this work, this price range could be on the high side, leading to a suboptimal strategy. Therefore, lower ranges for P will be considered.

3.3 Ensemble optimization of in-depth water diversion

Maximization of the objective function is an iterative process in which incremental adjustments of the control values are proposed in each iteration that should provide a consistent increase of the objective function. An efficient way to achieve this is to exploit the objective function gradient, which contains the sensitivities of objective function with respect to all controls. For cases in which no exact gradients are available, which is very likely to be the case for the controls describing the IDD process, approximate gradients or global search methods need to be employed. If the model is uncertain, as in the case of oil production, ensemble-based approximate gradients methods have been found to be efficient. This method was originally suggested by Chen et al. (2009) and later improved by Fonseca et al. (2014b).

The controls are gathered in a vector $\boldsymbol{u}$ of length n. If the control vector consists of time series of well rates or pressures for all wells, n may be very large. This study focuses on demonstrating the use of ensemble optimization for optimization of IDD strategies, and will therefore consider a single injection well with concentration, timing and duration of silicate injection as controls (i.e. $n = 3$)

$$\boldsymbol{u} = [u_{\text{concentration}}, u_{\text{timing}}, u_{\text{duration}}]. \tag{36}$$

Figure 1 illustrates the general injection strategy including the controls, where u_{timing} is given by t_0 and u_{duration} by Δt. The blue color indicates water injection (zero silicate concentration), while the green color indicates a non-zero silicate concentration. Injection rates will be constant in this study, but this simplification can be relaxed, adding separate rate controls for each time interval.

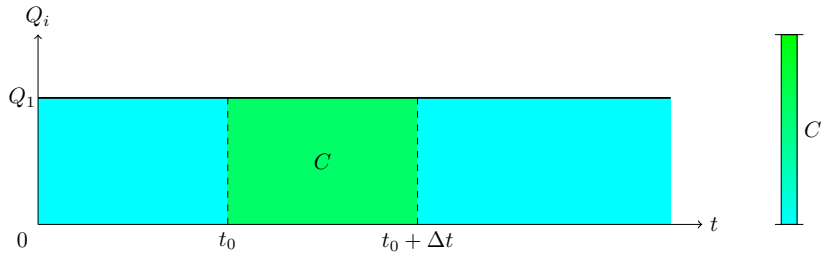

Figure 1 *Sodium silicate injection with a constant injection rate*

In each optimization iteration k, an ensemble of control vectors is created by perturbation of the current control solution and stored in the matrix U. The perturbed control vector $\boldsymbol{u}_k^i$ and the unperturbed control vector $\boldsymbol{u}_k$ both have length N. Each perturbed control is used as input for a model simulation, resulting in a perturbed objective function value $J(\boldsymbol{u}_k^i)$, where $i = \{1,\ldots,m\}$ with m the ensemble size. Objective function anomalies, constructed as the difference with the objective function for the unperturbed controls, are then stored in vector $\boldsymbol{j}$ as discussed in section 2.

If the model is uncertain, an ensemble of m model realizations can be used. In that case, the unperturbed controls can be applied to all model realizations to compute an expected objective function value. Such optimization under uncertainty is referred to as the robust optimization.

In this study, a simple trust region optimization scheme is used to update the controls with the gradient information to maximize objective function value. The trust region method makes use of a model function f that approximates the behaviour of the objective function near the point $\boldsymbol{u}_k$. For the model, the first order Taylor expansion of the objective function around $\boldsymbol{u}_k$ will be used, and look for a control update $\boldsymbol{u}_k + \boldsymbol{s}$ that lies inside the trust region.

The gradient is susceptible to noisy and small gradient components. To reduce this effect, the trust step is reset to zero if component g_i is close to zero.

$$s_i = \begin{cases} \min\left[\left(u_i^{\max} - u_i\right), \tau\left(u_i^{\max} - u_i^{\min}\right)\right] & \text{if } g_i > 0 \\ \max\left[\left(u_i^{\min} - u_i\right), -\tau\left(u_i^{\max} - u_i^{\min}\right)\right] & \text{if } g_i < 0 \\ 0 & \text{if } g_i = 0. \end{cases} \tag{37}$$

If the original search direction is positive, then the new search direction will be the minimum of the distance to the bounds, and the trust-size factor should be multiplied by the difference between the maximum and the minimum of the control. If it is negative, then it will be the maximum.

4 Numerical results

In this section, the simulation setup is described and its sensitivity to the model parameters is investigated. Next, optimization for deterministic and stochastic models is applied. The layered reservoir model is discussed first and then followed with a five-spot channelized model, both taking uncertainty into account using an ensemble of model realizations.

4.1 2D layered model

A simple 2D model will be used to test the workflow for IDD optimization. The model represents a vertical reservoir cross section connecting a vertical injector, positioned on one end, and a vertical producer on the opposite end. Different geological scenarios are used for the location of one or more high-permeable layers that provide a preferred pathway for injected water. In the first scenario, a single layer with a permeability of 400 mD connects injector and producer in the middle of the domain. The remaining background area has a much lower permeability of 50 mD. Additional parameters are listed in Table 2.

Property	Value
Δx, Δy, Δz	1 m, 100 m, 20 m
dimensions	256, 1, 5
$k_{background}$	50 mD (layers 1, 2, 4 and 5)
$k_{channel}$	400 mD (layer 3)
ϕ	0.2
Q_{inj}	564 m^3/day
BHP_{prd}	390 bar

Table 2 *Parameters of the 2D model and waterflooding strategy as used in the first numerical experiments.*

A base case recovery strategy is defined for the reference as a conventional waterflooding, i.e. without implementation of sodium silicate injection. The instantaneous and cumulative oil production rates for the base case strategy are indicated by the dashed lines in Figure 2 and Figure 3 respectively.

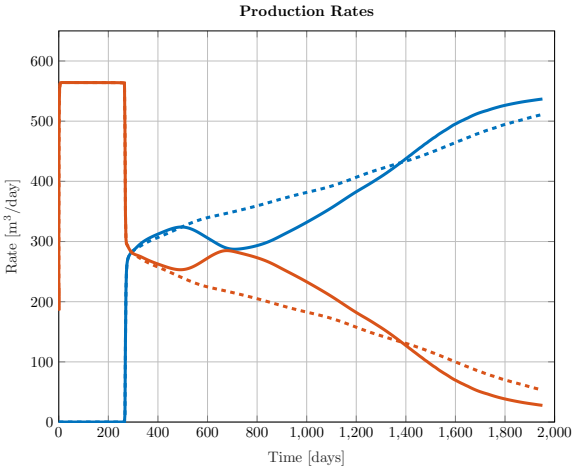

Figure 2 *Rates: oil (red), water (blue). With silicate (solid) or without (dashed)*

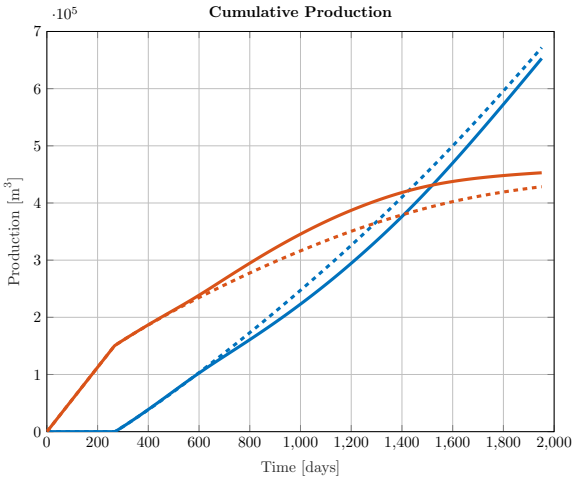

Figure 3 *Cumulatives: oil (red), water (blue). With silicate (solid) or without (dashed)*

After approximately 260 days water breaks through in the producing well. After 2000 days, oil production has significantly decreased and the water cut has increased to a level that would make further

production uneconomic. A reasonable reactive approach might be to start sodium silicate injection after water breakthrough. A 4wt% silicate solution was injected for 350 days, resulting in a total slug volume of 200,000 m^3 and a permeability reduction of 80% (Figure 4). This strategy is indicated by the solid line in Figure 2 and Figure 3.

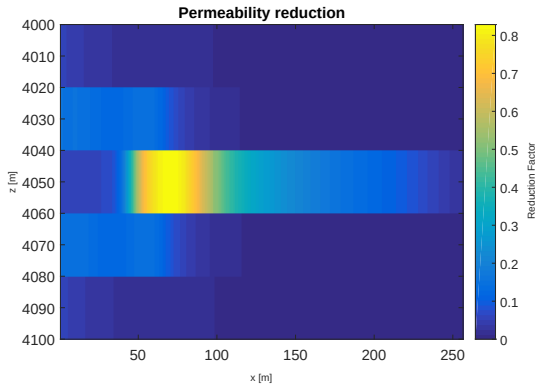

Figure 4 *Permeability reduction factor (color scale)*

The permeability reduction factor at the plug position is around 80% (Figure 4) and the resulting incremental oil production relative to the base strategy is 5.7%.

4.1.1 Sensitivity to resolution

Before attempting to find optimal strategies for IDD, first the sensitivity of simulations results to the spatial and temporal resolution is investigated for simulation of the IDD process. If sensitivity is large, performing simulations at very high spatial and temporal resolution is necessary that makes practical optimization infeasible for larger and more realistic models.

Simulations for different resolutions of grid cell size Δx were performed with a fixed time step of 1 day (Figure 5). Figure 6 shows the relative error in the oil production rate for the tested spatial resolutions. The error in production increases around the time of water breakthrough and towards the end of the production period. Figure 5 however suggests that rate errors are relatively moderate in absolute terms and that the highest relative errors occur when absolute rates are low, and should not strongly affect the total recovery.

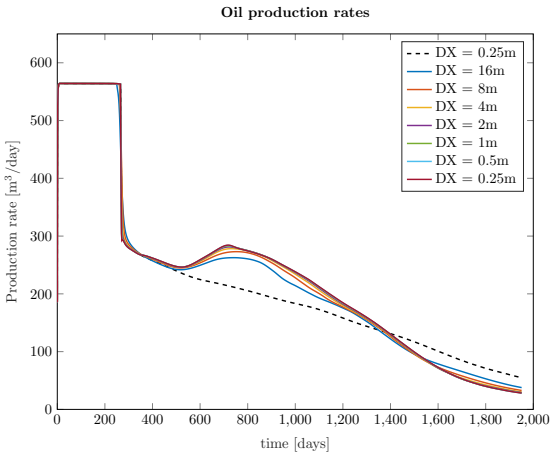

Figure 5 *Oil production rates for varying spatial grid resolution*

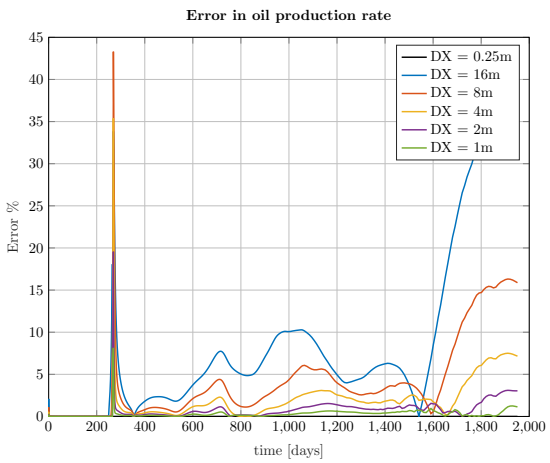

Figure 6 *Error in oil production rate for varying spatial grid resolution.*

This is confirmed by Figure 7 and Figure 8 that show both the sensitivity of oil recovery and permeability reduction to spatial and temporal resolution. Both quantities are affected by less than around 2% for the considered ranges of scales.

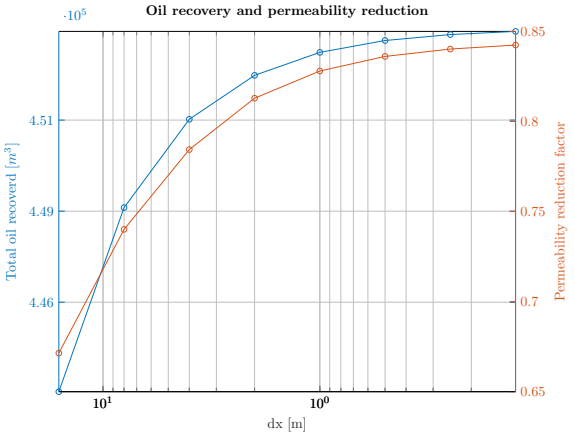

Figure 7 *Cumulative oil recovery and permeability reduction as a function of grid resolution for $\Delta t = 1$ day.*

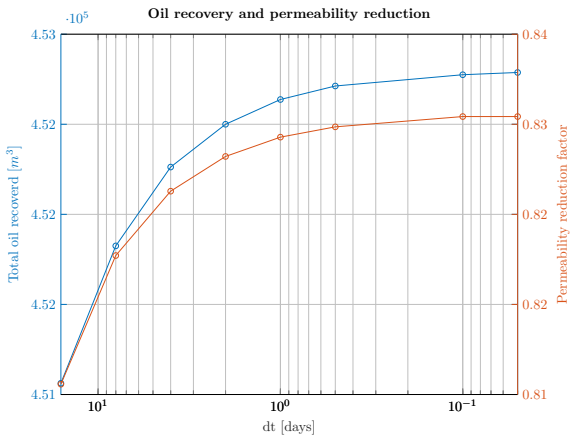

Figure 8 *Cumulative oil recovery and permeability reduction as a function of time resolution for $\Delta x = 1$ m.*

Further illustrations of the effect of spatial and temporal resolution are shown in Figure 9 to Figure 12 which consider the location of plug forming and the effect of resolution in simulation time. The distance from the injector to the plug was taken at the cell location with the maximum amount of precipitate. Figure 9 and Figure 10 show a decreasing distance for higher resolution. Total simulation time increases rapidly for spatial scales below $\Delta x = 1$ m.

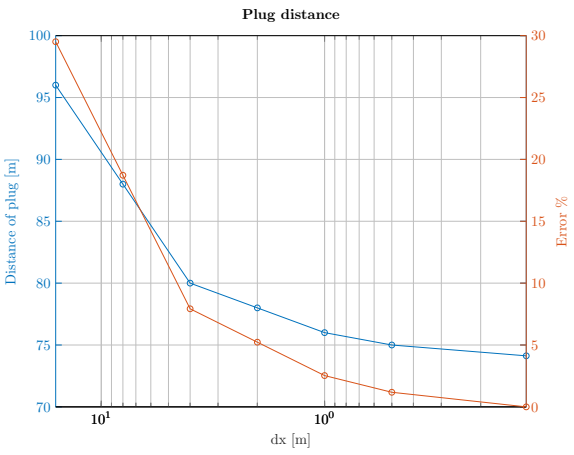

Figure 9 *Distance of plug from injector as a function of grid resolution for $\Delta t = 1$ day.*

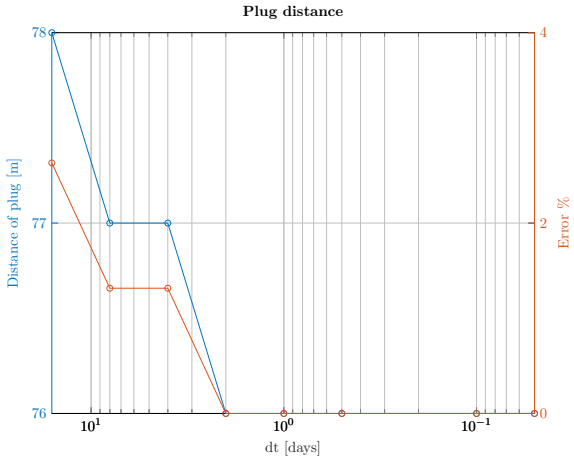

Figure 10 *Distance of plug from injector as a function of time resolution for $\Delta x = 1$ m*

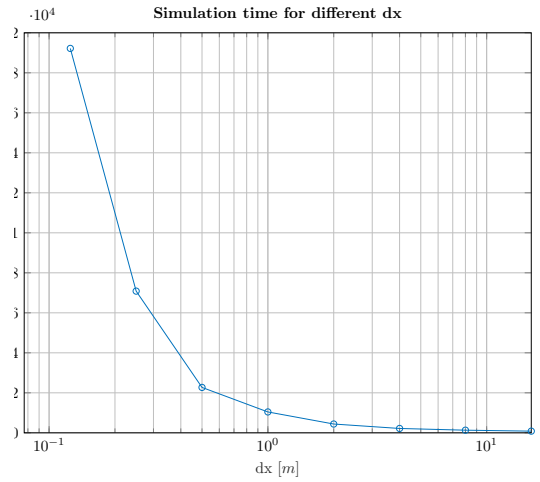

Figure 11 *Simulation time as a function of Δx. Resolution in time is $\Delta t = 1$ day.*

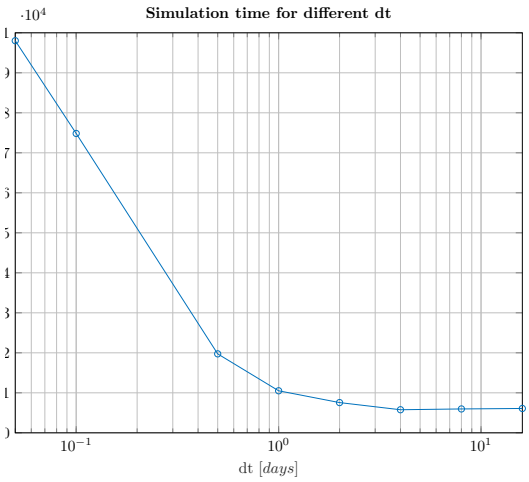

Figure 12 *Simulation time as a function of Δt. Resolution in space is $\Delta x = 1$ m.*

Based on the results from the sensitivity experiments, it can be concluded that a relatively coarser grid (than $\Delta x = 1$ m) and relatively larger time steps (than $\Delta t = 1$ days) are acceptable for forward simulation.

4.2 Case 1. Deterministic optimization for a single high-permeable layer

A deterministic optimization with both silicate solution injection timing t_0 and duration Δt as controls was performed for the 2D model, with a fixed concentration of 4wt% and a price of sodium silicate $r_{ci} = 17$ USD/m^3. Undiscounted cash flow was used as the objective function. The control sample size used for evaluating the gradient is 20 samples and the pertubation sigma $[\sigma_t, \sigma_{\Delta t}] = [20, 10]$. Controls were updated with a maximum of 3 inner iterations and the trust region algorithm. The optimization stopped when the maximum of 20 outer iterations was reached or when there was no more significant improvement in objective function value for 3 outer iterations. To verify the results of the optimization, first an exhaustive search was conducted by evaluating multiple combinations of these two control parameters (Figure 13). The optimum was found for $[t, \Delta t] = [200, 150]$. Next, an ensemble-based optimization was performed with an initial control combination of $[t, \Delta t] = [1400, 550]$. The optimization process is indicated by the arrows in Figure 13 where every green point corresponds to a control update. The red dot is the end result of the optimization and this optimum was found at $[t, \Delta t] = [176, 136]$ with an NPV of $4.5174 \cdot 10^7$ USD which is very close to the highest value found by exhaustive search.

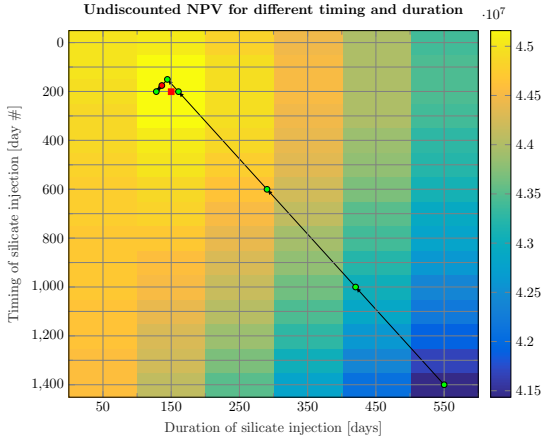

Figure 13 *Undiscounted J (color scale) and control updates (arrows and points) resulting from deterministic optimization.*

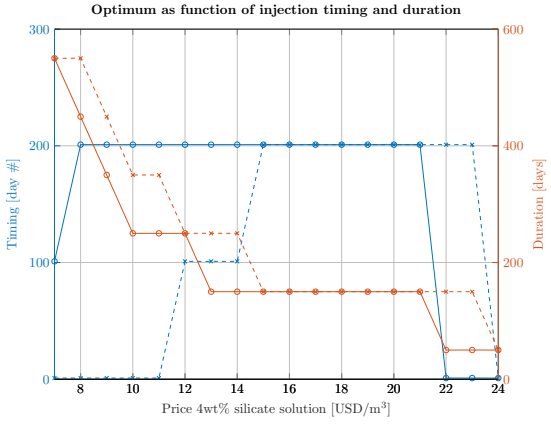

Figure 14 *Optimal control strategies for optimization of undiscounted (solid) and discounted (dashed) NPV.*

Since the optimum depends largely on the silicate solution price, Figure 14 shows the optimum combinations of $[t, \Delta t]$ as function of price for both undiscounted and 8% discounted NPV, where $t \in [0, 1400]$ and $\Delta t \in [50, 550]$. The strategy is similar for the price of sodium silicate between 15 and 21 USD/m^3, but between 8 and 15 USD/m^3 the discounted case benefits from injecting earlier.

4.3 Case 2. Deterministic optimization for a heterogeneous reservoir

Up to now, the presence of a single high-permeabile layer is known connecting the injecting and producing wells. In reality, one may encounter situations with different, mostly uncertain, geology. Since in that case constructing a model that is a perfect representation of the subsurface is not possible, it is better to construct an ensemble of models that are all equally probable as the description of the subsurface reservoir. It may be expected that each geological scenario would result in a different response of the subsurface system to the same control strategy.

In order to test this assumption, a slight modification of the original setup is considered. It is assumed that high-permeable layers are present in the reservoir that create a partial connection between the two wells. The layers are disconnected in the middle part of the reservoir cross-section. This study assumes that the reservoir contains additional high-permeable features with only approximately known extensions in lateral distance, representing for example, channel beds.

One of such scenarios is shown in Figure 15. In this model, $K_x = K_y$ and $K_z = {}^1/_{10} \cdot K_x$ and $K_x = 1000$ mD in the high permeable features, and K_x is either 50 or 1 mD in the low-permeable parts of the reservoir. The size of the model is 200m x 100m x 100m with grid dimensions of 1m x 100m x 10m and uniform porosity of 0.2. First a normal waterflood was performed. After 2000 days with an injection rate of 500 m^3/day and producer BHP of 390 bar, there are 3 areas visible with high remaining oil saturation (Figure 16). The NPV, predicted with this waterflood strategy, is \$14 millions.

Optimizations were performed with different prices P for dry sodium metasilicate (equation 35) where the silicate concentration is added as a third control. The control sample size used for evaluating the gradient is now 40 samples and the pertubation sigma $[\sigma_t, \sigma_{\Delta t}, \sigma_C] = [50, 20, 1]$. Controls were updated with a maximum of 3 inner iterations using trust region algorithm. The optimization stopped when the maximum of 30 outer iterations was reached or when there was no more significant improvement in objective function value (NPV). Results are here reported obtained with a value of $P = 100$ \$/m^3 for which the optimal strategy achieves an undiscounted NPV of \$23 million, which represents a 64% increase over the waterflood scenario. The optimal strategy is to inject water for 438 days before starting injection of a 7.44 wt% silicate solution for 744 days ($[t, \Delta t, C] = [438, 744, 7.44]$). Since the injection rate is fixed at 500 m^3/day, the total volume of injected silicate solution is 372,000 m^3. The plug was formed 90 meters away from the injector, as indicated by the red circle in Figure 17. At this location, the largest permeability reduction was observed.

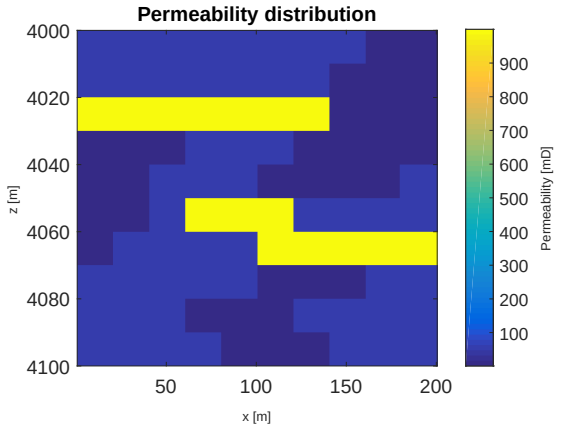

Figure 15 *Permeability K_x before injection of sodium silicate.*

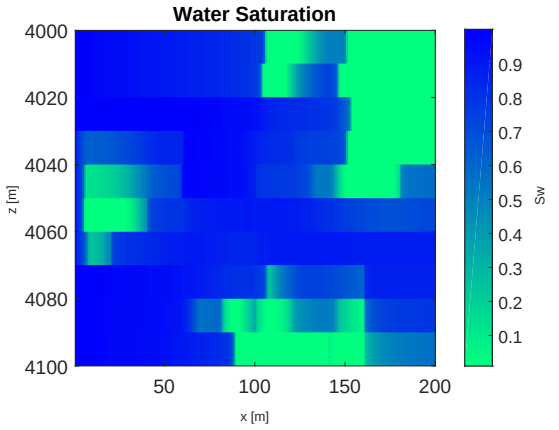

Figure 16 *Water saturation at the end of the waterflood reference strategy.*

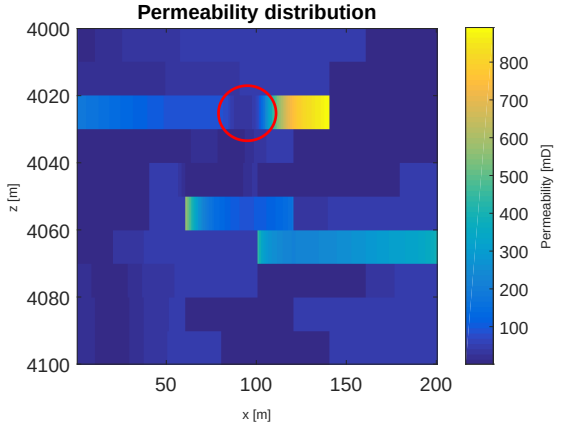

Figure 17 *Permeability K_x at the end of the IDD strategy. The red circle indicates the plug position.*

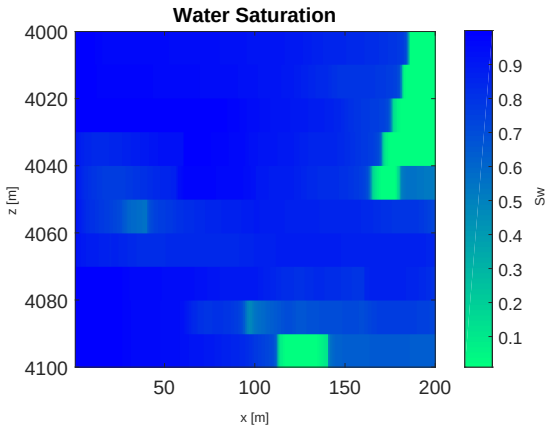

Figure 18 *Water saturation at the end of the IDD strategy.*

Figure 18 shows that less oil is left behind than in the base waterflood case without sodium silicate injection (Figure 16). Oil production is identical for most of the first 520 days in the case with and without silicate solution injection, as indicated by the solid and dashed lines in Figure 19 and Figure 20 respectively. After this period, an increase in oil production and a decrease in water production can be clearly observed.

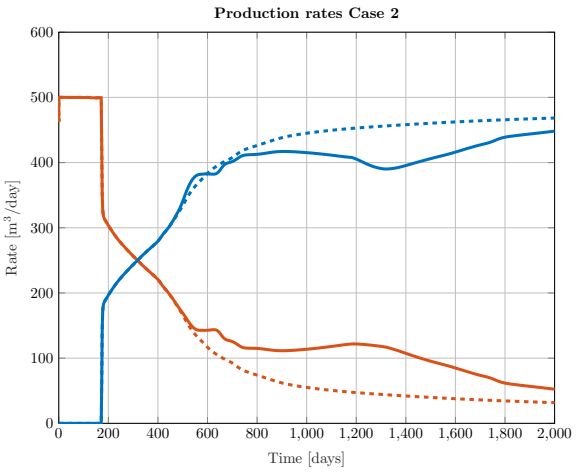

Figure 19 *Oil rate (red) and water rate (blue). With silicate (solid) and without (dashed)*

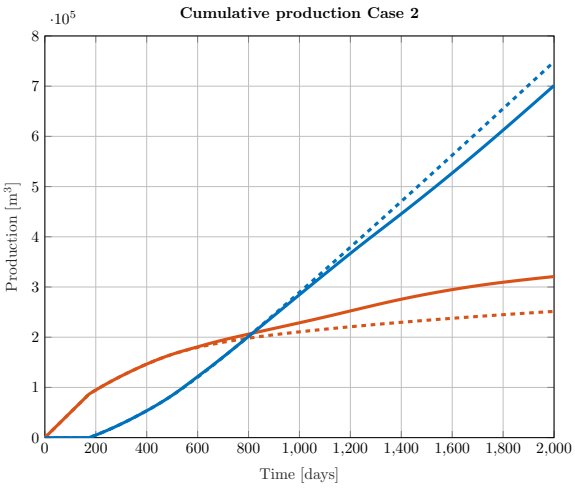

Figure 20 *Cumulative oil rate (red) and water rate (blue). With silicate (solid) and without (dashed)*

The starting control values for the optimization were $[t, \Delta t, C] = [1, 0, 0]$, which corresponds to a waterflood without silicate injection. The bounds for the controls were set to $t \in [1, 2000]$, $\Delta t \in [1, 1000]$ and $C \in [0, 10]$. It took 13 iterations to reach the optimum (Figure 21). Note, that the intermediate result at iteration 5 suggests that the optimization is close to a local optimum strategy in which the silicate solution is injected from day 1. Further iterations ultimately resulted in a significant increase in objective function by delaying this injection.

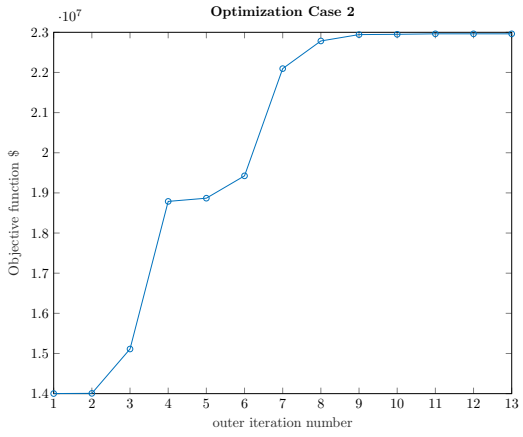

Figure 21 *IDD optimization with $P = 100\ \$/m^3$. Objective function is undiscounted NPV in $.*

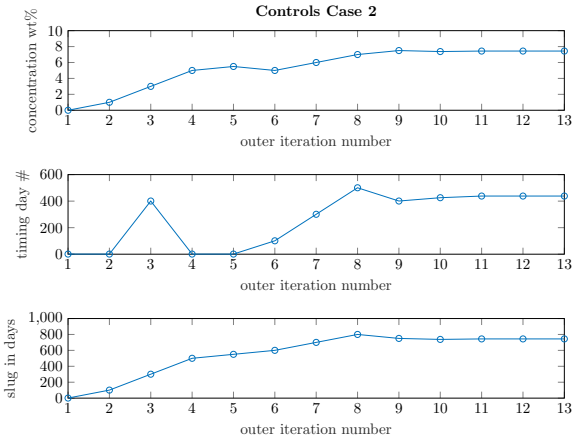

Figure 22 *Control updates during iterations of the Case 2 optimization.*

In order to verify the optimization result, the objective functions values were also evaluated for regular distributed samples in the control domain, which now has dimension 3 (Figure 23). The optimum is indicated by a red dot. There are small differences in the controls and NPV with the optimum found by optimization. This could suggest a very smooth objective function space with similar NPV for different control combinations. From the differences with the first optimization case, it is clear that a single operating strategy, optimal for all possible geological scenario's, does not exist for this process. One choice in such case is to optimize the expected recovery or NPV, as evaluated over all available geological realizations.

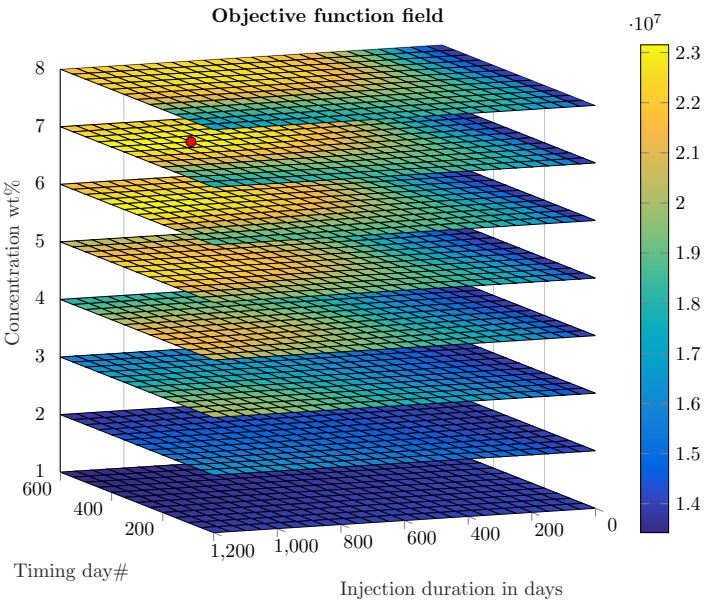

Figure 23 *Objective function values (undiscounted NPV in $.) at regular control intervals. The optimal value is indicated by the red dot.*

4.4 Case 3. Robust optimization for a heterogeneous reservoir

In the third case discussed here, it is assumed that geological uncertainty is characterized by an ensemble of 40 equally probable geological models (Figure 25) where the length and position of high permeable paths follow a normal distribution. The ratio is 1:1 for the control sample perturbations to the number of geological models within the ensemble. This means $N_p = 1$ and $M = 40$, resulting in less computational costs to do one estimation of the gradient. The initial guess for optimization is $[t, \Delta t, C] = [1, 1, 8]$ (start injection of a 8 wt% solution at day 1 with an injection duration of 1 day) and the control sigma $[\sigma_t, \sigma_{\Delta t}, \sigma_C] = [50, 50, 0.5]$. The optimal strategy from the robust optimization is $[t, \Delta t, C] = [482, 379, 6.41]$. The expected objective function value resulting from this optimal strategy is 21.3 million USD, which represents an increase of 40% over the initial strategy.

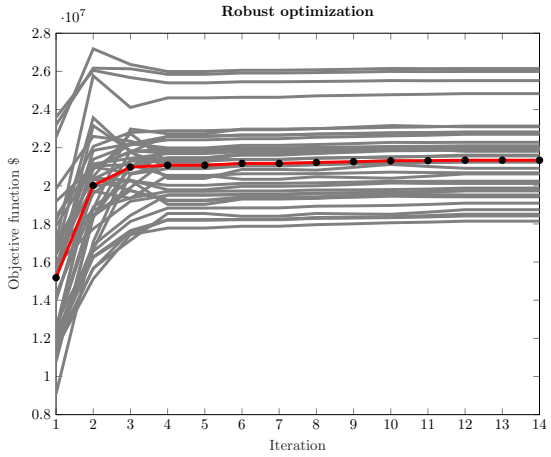

Figure 24 *Robust optimization process for an ensemble of 40 of model realizations. Grey lines indicate individual ensemble members, and the red line represents the ensemble mean.*

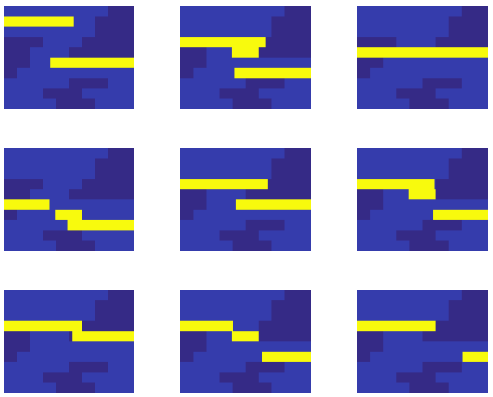

Figure 25 *Nine arbitrary permeability models taken from the ensemble of 40 model realizations.*

4.5 Case 4. Robust optimization for a channelized five-spot reservoir

In the fourth case, robust optimization is applied to a five spot channelized model. de Hoop et al. (2018) originally generated ensembles of channelized model realizations with a specific paleoflow orientation in a low permeable background, using Multi Point Statistics (MPS) and training image data (Strebelle (2002)) for multiple grid dimensions each. Within the ensemble, the model size was reduced to a quarter of the original and wells were repositioned, allowing the possibility for water breakthrough in all four producers within a reasonable time frame. In the five-spot model channels have a high permeability of

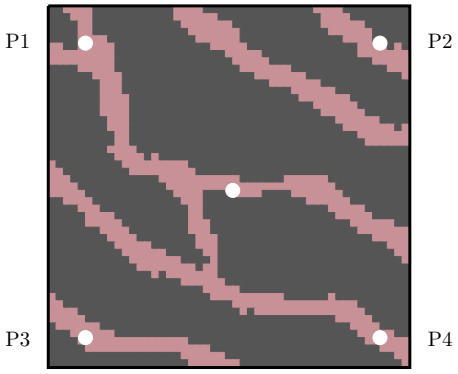

Figure 26 *One of the ensemble members. The paleoflow orientation is southwest-northeast*

1000mD with 30% porosity, but background shale is with 5mD much less permeable and it also has a lower porosity of 10%. The size of the model is 500m x 500m x 10m with grid dimensions of 10m x 10m x 10m running in the x- and y-direction. One injector in the middle is rate controlled at 100 m^3/day and four producers are controlled by BHP set at 390 bar.

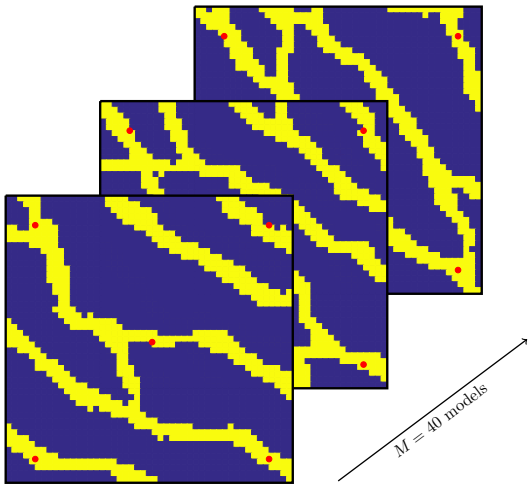

Figure 27 *The ensemble size is 40 geological models. The main uncertainty lies in the position of channel sand*

Uncertainty in the underlying model parameters, in this case porosity and permeability, is then reflected by the ensemble of model realizations. Figure 27 illustrates the ensemble of model realizations for a five-spot well configuration, where the ensemble size is 40 geological models. All members of the ensemble have the same paleoflow orientation and same well positions, where wells are constrained to channel sand. This means neither injector nor producer is placed in shale. The average first water breakthrough time in one of the four producers is 562 days.

Controls were updated with a maximum of 3 inner iterations and the trust region algorithm. The optimization stopped when the maximum of 30 outer iterations was reached or when there was no more significant improvement in objective function value for 3 outer iterations. The control sigma corresponds to $[\sigma_t, \sigma_{\Delta t}, \sigma_C] = [100, 50, 0.5]$. The initial guess for optimization is $[t, \Delta t, C] = [250, 300, 8]$ (start injection of a 8 wt% solution after 250 days with an injection duration of 300 days). The optimal strategy from the robust optimization for an ensemble size of 40 is $[t, \Delta t, C] = [455, 783, 12.3]$.

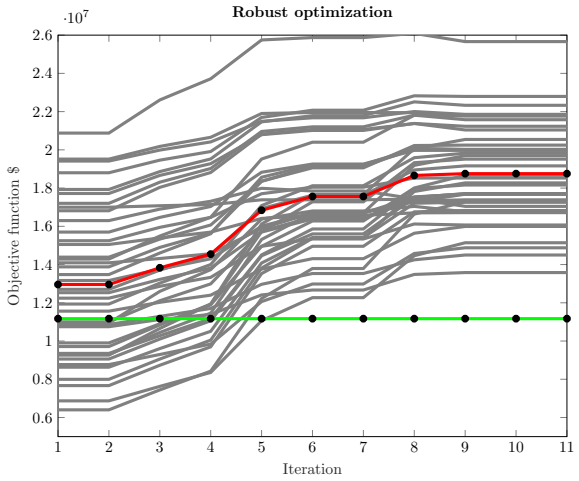

Figure 28 *Robust optimization for an ensemble of 40 of model realizations.*

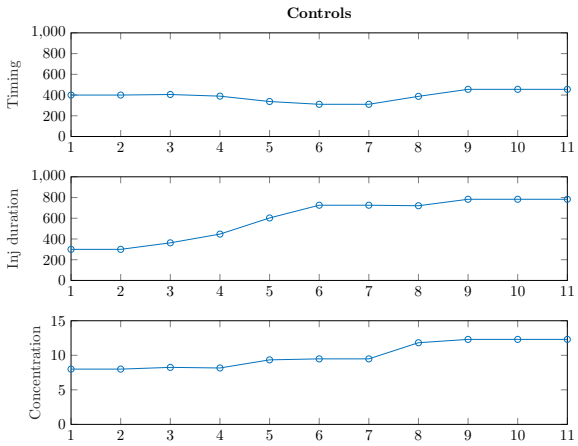

Figure 29 *Control updates during the iterations*

In Figure 28, the red line is the ensemble mean for the IDD optimization and the green line is the ensemble mean for a non reactive waterflood. The optimal IDD strategy gives a 60% increase in objective function over this non reactive waterflood strategy. The expected objective function value resulting from this optimal strategy is 18.6 million USD.

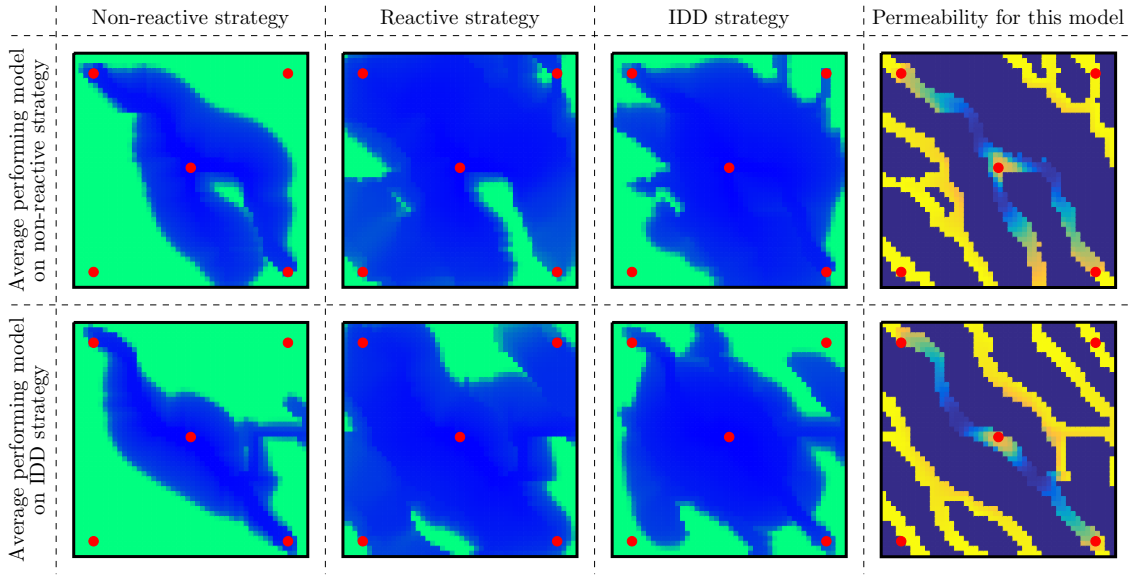

Figure 30 *Comparison of water saturation maps for three strategies: non-reactive waterflood, reactive waterflood and IDD. This was done for the average performing model on a non-reactive waterflood stategy (above) and on the average performing model on the IDD strategy (below). The permeability distribution map corresponds to the IDD strategy.*

In figure 30 water saturation is compared for three different strategies on two model realizations performing close to the ensemble average. Both models show better sweep efficiency for the optimal IDD strategy over a non-reactive waterflood. However, in the field it is common to shut in wells producing at uneconomic water cut, which could be a reasonable reactive strategy without any IDD implementation. The uneconomic water cut is determined at 86% water cut. Figure 30 suggests this strategy achieves better sweep efficiency over the optimal IDD strategy from robust optimization.

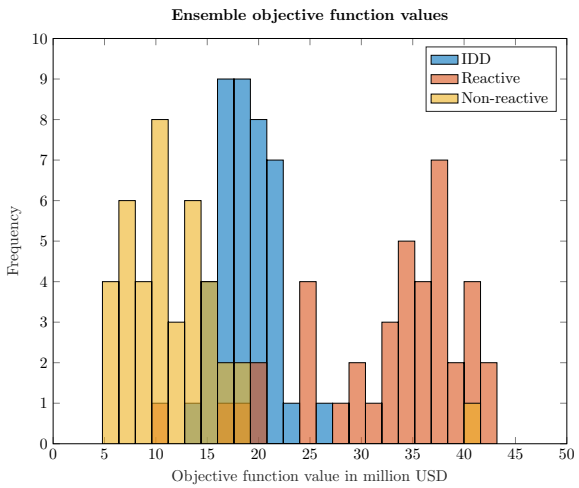

Figure 31 *Histogram of the ensemble objective function values.*

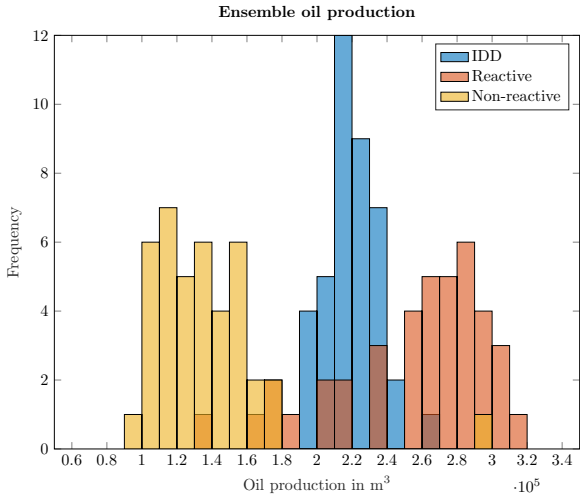

Figure 32 *Histogram of the ensemble oil production.*

Histograms in figures 31 and 32 show the distribution of the objective function value and oil production, indicating overall better results for the reactive approach. Up till now only one permeability configuration was used, where channel sand is 1000mD and shale is 5mD, resulting in a permeability ratio $K_{\text{channel}}/K_{\text{shale}}$ of 200. Exploring lower permeability ratios may lead to situations where IDD is preferred over this reactive approach.

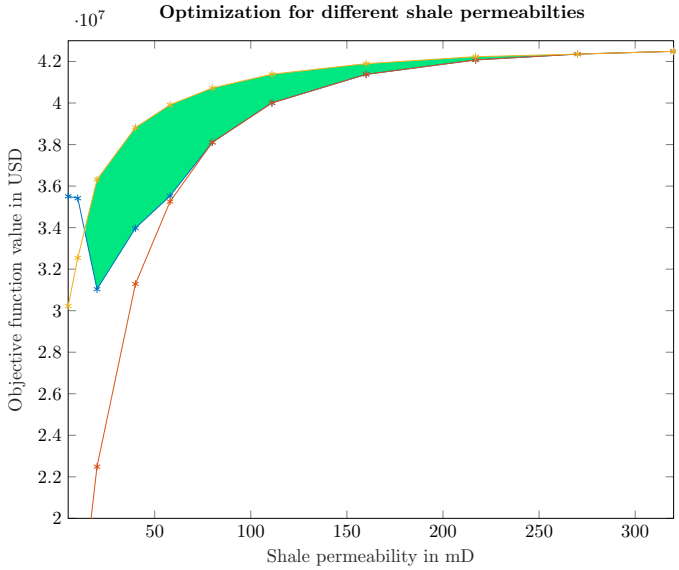

Figure 33 *NPV for the average performing model on the IDD strategy, as function of shale permeability. Optimal IDD strategy (yellow), waterflood (red). Reactive approach (blue): Shut in producer at water cut of 86%. Channel permeability remains the same (1000mD)*

Figure 33 compares the optimal IDD strategy found by the EnOpt, for each shale permeability, to the reactive approach and a waterflood. The lowest shale permeability is 5mD as used previously in the five-spot model and the highest is 320mD. Figure 33 suggests the reactive approach is only out-competing the IDD strategy for low shale permeabilities, whereas higher shale permeabilities may show the benefit of applying IDD indicated by the green area. It should be noted that this evaluation (as used for figure 33) was performed on only one model out of the ensemble, performing close to the average on the IDD strategy. Other ensemble members may behave differently.

4.5.1 Sensitivity to spatial resolution

Table 3 shows some sensitivities to changes in spatial resolution for one of the ensemble members. Here three areas with high permeability reduction were defined as the plug locations. In these areas the amount of moles of silicate formed was taken from the data, as well as the porosity reduction per volume of silicate. Additional sensitivities are the total amount of oil and water produced. The three simulations were performed with a BHP of 390 bars, injection rate of 200 m^3/day and time steps of 2 days

Cells $N_x \times N_y$	**Moles of silicate in plug**	**Maximum permeability reduction %**	**porosity reduction % per volume of silicate m^3**	**Channel area % below 100mD**	**Oil produced in m^3**	**Water produced in m^3**
50×50	$3.73 \cdot 10^6$	96	12.1	10.6	$2.31 \cdot 10^5$	$1.79 \cdot 10^5$
150×150	$4.08 \cdot 10^6$	98	12.6	11.1	$2.28 \cdot 10^5$	$1.81 \cdot 10^5$
250×250	$4.18 \cdot 10^6$	98	12.8	11.1	$2.28 \cdot 10^5$	$1.82 \cdot 10^5$

Table 3 *Sensitivity of model parameters to resolution changes for the five-spot model*

Total simulation time for the 50x50 model was 680 seconds, whereas the 150x150 model showed a significant increase with approximately 7 hours. The highest resolution model was of course most computationally expensive with a total simulation time of 47 hours.

5 Conclusions

This study implemented a fully coupled model to simulate the in-depth diversion (IDD) process. This study proposed the application of an ensemble-based gradient methodology for the IDD process. A simple 2D layered model was used to test the workflow for IDD optimization. A reasonable reactive approach where sodium silicate injection starts just after water breakthrough showed incremental oil production over a base case strategy, defined as a conventional waterflood without implementation of sodium silicate injection.

Limited sensitivity to both spatial and temporal resolution in a simple 2D setting was observed. An increase in relative error in oil production was observed around time of water breakthrough and towards the end of the production period, however rate errors are relatively moderate in absolute terms and the highest relative errors occur when absolute rates are low. Sensitivity of oil recovery and permeability reduction to spatial and temporal resolution confirmed that this observation does not strongly affect total recovery. Therefore a relatively coarse grid and relatively large time step are acceptable for forward simulation. This may be different in more complex and more heterogeneous cases.

Optimization of the IDD process resulted in improved objective function values, using injection timing, injection duration and concentration of the sodium silicate solution as controls. Different models were observed to result in different optimal strategies, which were not self-evident and differ from a typical reactive strategy. Given uncertainty in permeability, robust optimization was able to find an optimal strategy for an ensemble of 40 model realizations. Ensemble optimization therefore proves to be a viable approach to find optimal IDD strategies.

The application to larger and geologically more complex cases and extension with well rate and pressure controls is the topic for future research. Before making an attempt on this, slight changes can be made to the current models. Here it is recommended to explore the potential benefit of an IDD strategy over a reactive approach for other channel-shale permeability ratios. Another possibility would be to switch producers to injectors and vice versa in the five-spot model, which may lead to different IDD strategies. Other questions to be answered are related to upscaling and the issue of computational cost associated with higher resolutions required for more complex cases to accurately simulate this coupled process. This includes research to what extent upscaling is required to make the optimization computationally tractable and which efficient or effective upscaling strategies exist, and how they can be incorporated into the optimization workflow.

References

Chen, Y. [2008] *Ensemble-based closed-loop production optimization*. The University of Oklahoma.

Chen, Y., Oliver, D.S., Zhang, D. et al. [2009] Efficient ensemble-based closed-loop production optimization. *SPE Journal*, **14**(04), 634–645.

Farshidi, S., Fan, Y., Durlofsky, L. and Tchelepe, H.A. [2013] Chemical Reaction modeling in a compositional reservoir simulation framework. *SPE 163677*.

Fonseca, R., Leeuwenburgh, O., Van den Hof, P., Jansen, J.D. et al. [2014a] Improving the ensemble-optimization method through covariance-matrix adaptation. *SPE Journal*, **20**(01), 155–168.

Fonseca, R., Stordal, A., Leeuwenburgh, O., Van den Hof, P. and Jansen, J.D. [2014b] Robust ensemble-based multi-objective optimization. In: *ECMOR XIV-14th European conference on the mathematics of oil recovery*.

Fonseca, R.R.M., Chen, B., Jansen, J.D. and Reynolds, A. [2017] A stochastic simplex approximate gradient (StoSAG) for optimization under uncertainty. *International Journal for Numerical Methods in Engineering*, **109**(13), 1756–1776.

Garipov, T., Tomin, P., Rin, R., Voskov, D. and Tchelepi, H. [2018] Unified Thermo-Compositional-Mechanical Framework for Reservoir Simulation. *Computational Geosciences*.

Hamouda, A.A. and Amiri, H.A.A. [2014] Factors affecting alkaline sodium silicate gelation for in-depth reservoir profile modification. *Energies*, **7**(2), 568–590.

Hatzignatiou, D.G., Giske, N.H. et al. [2016] Water-Soluble Sodium Silicate Gelants for Water Management in Naturally Fractured Carbonate Reservoirs. In: *SPE Europec featured at 78th EAGE Conference and Exhibition*. Society of Petroleum Engineers.

Hiorth, A., Sagen, J., Lohne, A., Nossen, J., Vinningland, J., Jettestuen, E. and Sira, T. [2016] IORSim-A Simulator for Fast and Accurate Simulation of Multi-phase Geochemical Interactions at the Field Scale. In: *ECMOR XV-15th European Conference on the Mathematics of Oil Recovery*.

de Hoop, S., Voskov, D., Vossepoel, F. and Jung, A. [2018] Quantification Of Coarsening Effect On Response Uncertainty In Reservoir Simulation. In: *ECMOR XVI-16th European Conference on the Mathematics of Oil Recovery*.

Hou, J., Zhou, K., Zhang, X.S., Kang, X.D. and Xie, H. [2015] A review of closed-loop reservoir management. *Petroleum Science*, **12**(1), 114–128.

Icopini, G.A., Brantley, S.L. and Heaney, P.J. [2005] Kinetics of silica oligomerization and nanocolloid formation as a function of pH and ionic strength at 25 C. *Geochimica et Cosmochimica Acta*, **69**(2), 293–303.

Jansen, J. [2011] Adjoint-based optimization of multi-phase flow through porous media–a review. *Computers & Fluids*, **46**(1), 40–51.

Kennedy, J. [2011] Particle swarm optimization. In: *Encyclopedia of machine learning*, Springer, 760–766.

Leeuwenburgh, O. [2017] Ensemble methods for optimization of subsurface flow. In: *Lecture notes AES1490 Delft University of Technology*.

Mayer, E., Berg, R., Carmichael, J., Weinbrandt, R. et al. [1983] Alkaline injection for enhanced oil recovery-A status report. *Journal of Petroleum Technology*, **35**(01), 209–221.

Metropolis, N., Rosenbluth, A.W., Rosenbluth, M.N., Teller, A.H. and Teller, E. [1953] Equation of state calculations by fast computing machines. *The journal of chemical physics*, **21**(6), 1087–1092.

Skrettingland, K., Dale, E.I., Stenerud, V.R., Lambertsen, A.M., Nordaas Kulkarni, K., Fevang, O., Stavland, A. et al. [2014] Snorre In-depth Water Diversion Using Sodium Silicate-Large Scale Inter-well Field Pilot. In: *SPE EOR Conference at Oil and Gas West Asia*. Society of Petroleum Engineers.

Skrettingland, K., Giske, N.H., Johnsen, J.H., Stavland, A. et al. [2012] Snorre in-depth water diversion using sodium silicate-single well injection pilot. In: *SPE Improved Oil Recovery Symposium*. Society of Petroleum Engineers.

Skrettingland, K., Ulland, E., Ravndal, O., Tangen, M., Kristoffersen, J., Stenerud, V., Dalen, V., Standnes, D., Fevang, Ø., Mevik, K. et al. [2016] Snorre In-Depth Water Diversion-New Operational Concept for Large Scale Chemical Injection from a Shuttle Tanker. In: *SPE Improved Oil Recovery Conference*. Society of Petroleum Engineers.

Spall, J.C. [1998] Implementation of the simultaneous perturbation algorithm for stochastic optimization. *IEEE Transactions on aerospace and electronic systems*, **34**(3), 817–823.

Stavland, A., Jonsbråten, H., Vikane, O., Skrettingland, K. and Fischer, H. [2011] In-depth water diversion using sodium silicate–Preparation for single well field pilot on Snorre. In: *IOR 2011-16th European Symposium on Improved Oil Recovery*.

Strebelle, S. [2002] Conditional simulation of complex geological structures using multiple-point statistics. *Mathematical geology*, **34**(1), 1–21.

Trujillo, R. [2017] *In-depth water diversion strategies*. Msc thesis, Delft Univeristy of Technology.

Trujillo, R., Voskov, D. and Leeuwenburgh, O. [2018] Simulation of In-depth Water Diversion Using Sodium Silicate. In: *43rd Workshop on Geothermal Reservoir Engineering*.

Voskov, D.V., Henley, H. and Lucia, A. [2017] Fully compositional multi-scale reservoir simulation of various CO2 sequestration mechanisms. *Computers and Chemical Engineering*, **96**, 183 – 195.

Voskov, D.V. and Tchelepi, H.A. [2012] Comparison of nonlinear formulations for two-phase multi-component EoS based simulation. *Journal of Petroleum Science and Engineering*, **82**, 101–111.

Zaydullin, R., Voskov, D., James, S., Henley, H. and Lucia, A. [2014] Fully compositional and thermal reservoir simulation. *Computers & Chemical Engineering*, **63**, 51–65.